ACS OMEGA

http://pubs.acs.org/journal/acsodf

Article

PpIX/IR-820 Dual-Modal Therapeutic Agents for Enhanced PDT/PTT Synergistic Therapy in Cervical Cancer

Ting Yan, Gulinigaer Alimu, Lijun Zhu, Huimin Fan, Linxue Zhang, Zhong Du, Rong Ma, Shuang Chen, Nuernisha Alifu,* and Xueliang Zhang*

Cite This: *ACS Omega* 2022, 7, 44643−44656

Read Online

ACCESS | Metrics & More | Article Recommendations | Supporting Information

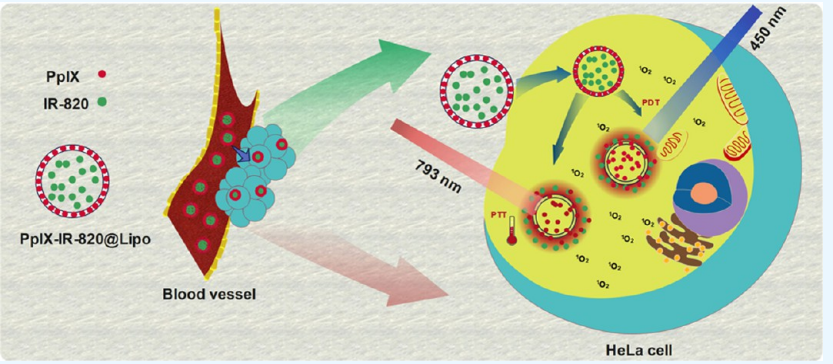

ABSTRACT: High treatment accuracy is the key to efficient cancer treatment. Photodynamic therapy (PDT) and photothermal therapy (PTT) are two kinds of popular, precise treatment methods. The combination of photodynamic and photothermal therapy (PDT/PTT) can greatly enhance the precise therapeutic efficacy. In this work, protoporphyrin IX (PpIX) was selected as the PDT agent (photosensitizer), and new indocyanine green (IR-820) was selected as the PTT agent. Further, the two kinds of theranostic agents were encapsulated by biological-membrane-compatible liposomes to form PpIX-IR-820@Lipo nanoparticles (NPs), a new kind of PDT/PTT agent. The PpIX-IR-820@Lipo NPs exhibited good water solubility, a spherical shape, and high fluorescence peak emission in the near-infrared spectral region (700−900 nm, NIR). The cellular toxicity of PpIX-IR-820@Lipo NPs for human cervical cancer cells (HeLa) and human cervical epithelial cells (H8) was detected by the CCK-8 method, and low cytotoxicity was observed for the PpIX-IR-820@Lipo NPs. Then, the excellent cellular uptake of PpIX-IR-820@Lipo NPs was confirmed by laser scanning confocal microscopy. Moreover, the PDT/PTT property of PpIX-IR-820@Lipo NPs was illustrated via 2′,7′-dichlorofluorescin diacetate (DCFH-DA) and annexin V-fluorescein isothiocyanate (annexin V-FITC), as indicator probes. The PDT/PTT synergistic efficiency of PpIX-IR-820@Lipo NPs on HeLa cells was verified, exhibiting a high efficiency of 70.5%. Thus, the novel theranostic PpIX-IR-820@Lipo NPs can be used as a promising PDT/PTT synergistic theranostic nanoplatform in future cervical cancer treatment.

1. INTRODUCTION

Cervical cancer, a common cancer in women, has a high incidence rate.[1] Now routine clinical treatments for cervical cancer include surgery, radiotherapy, and chemotherapy.[2−4] Commonly used auxiliary diagnostic methods include lymphangiography, ultrasound, computed tomography (CT), and magnetic resonance imaging (MRI).[5] Unfortunately, most of these methods have side effects and low sensitivity.[6] Thus, there is great demand for new methods of diagnosis and treatment.

Photodynamic therapy (PDT) and photothermal therapy (PTT) are two kinds of highly effective and precise tumor treatment.[7,8] PDT has attracted tremendous attention for its high localized efficiency and the little damage it does to surrounding normal tissue.[9] PDT includes three essential components: excitation light, photosensitizers (PSs), and reactive oxygen species (ROS).[10,11] Studies showed that during the PDT process, the PS could generate high ROS under reasonable excitation light, which could kill tumor cells.[12−14] Among the commonly used PSs, PpIX is favorable for its strong photosensitive activity, low toxicity, and fast metabolism.[15,16] Chudal et al.[17] designed and synthesized a nanoplatform (PpIX-Lipo-MnO_2) based on PpIX. The PDT

Received: May 13, 2022
Accepted: August 10, 2022
Published: September 15, 2022

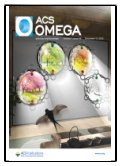

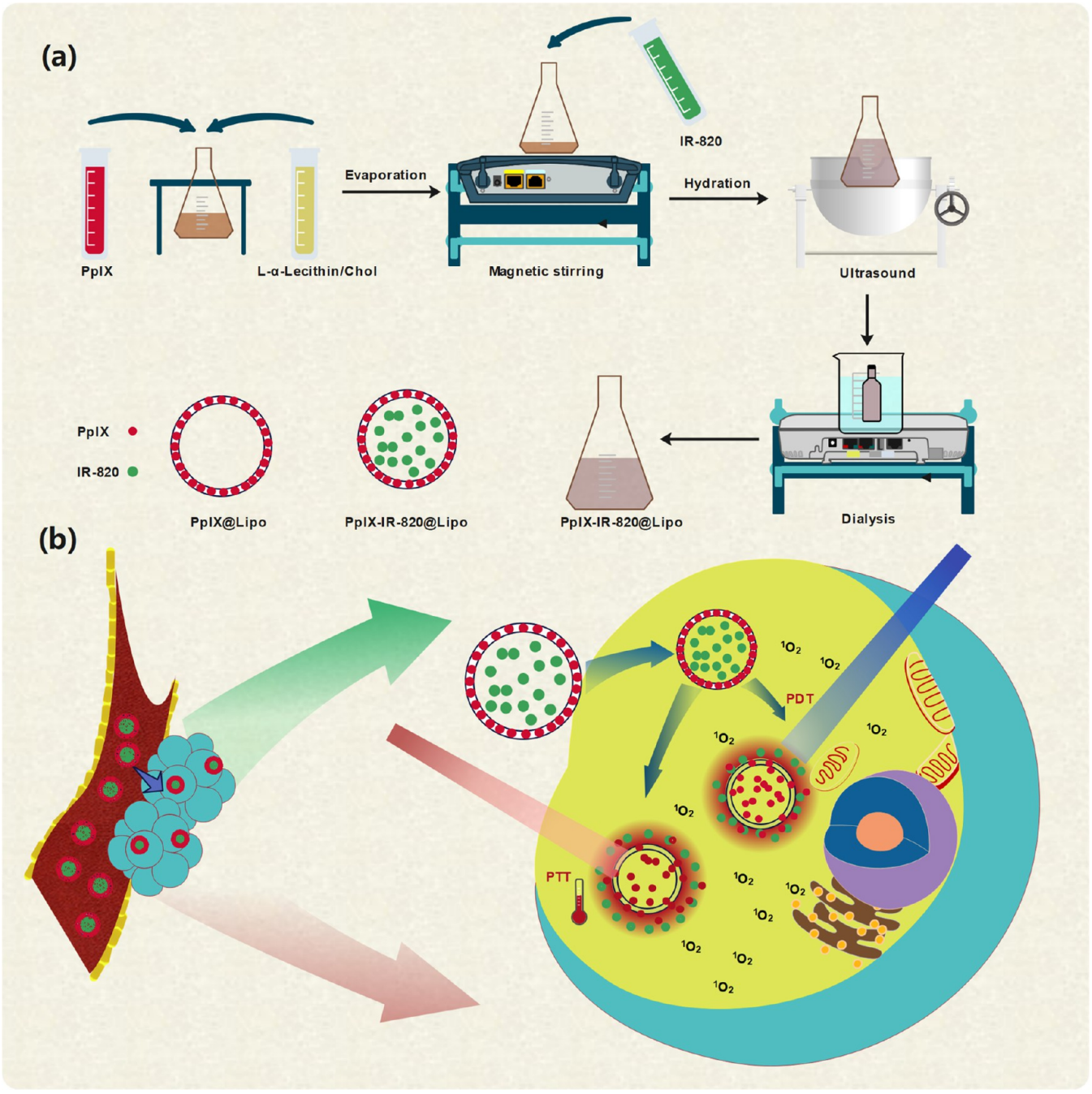

Figure 1. (a) Schematic illustration of the synthesis route for PpIX-IR-820@Lipo NPs and (b) photodynamic−photothermal therapy in tumor cells.

efficiency of the PpIX-Lipo-MnO_2 nanoparticles (NPs) could be enhanced greatly by converting common H_2O_2 into oxygen.

Another ideal tumor treatment is PTT, which is noninvasive, repeatable, and safe.[18,19] The photothermal agent could convert light energy into hyperthermia under laser irradiation and then induce the ablation of tumor cells.[20−22] New indocyanine green (IR-820) is a new kind of photothermal agent with excellent photochemical properties, strong near-infrared (NIR) fluorescence emission, and stability.[23,24] In our previous report,[25] IR-820 was encapsulated with the amphiphilic polymer matrix PSMA (IR-820@PSMA), and high PTT with excellent stability was achieved. The combination of PTT and PDT may be used to obtain high therapeutic efficiency, potentially making it an ideal treatment method. A better way to combine PDT/PTT is to encapsulate the PS and the photothermal agent in one NP.

Liposomes are artificial membranes composed of lecithin and cholesterol, which can encapsulate hydrophilic and hydrophobic drugs effectively.[26,27] They are favorable nanocarriers for similar structures of cell membranes.[28] Chen et al.[29] designed indocyanine green (ICG) and doxorubicin (DOX) encapsulated tumor-triggered targeting ammonium bicarbonate (TTABC) liposomes (ICG&DOX@TTABC) to achieve chemo/photothermal/photodynamic multimodal therapy. The ICG&DOX@TTABC could specifically accumulate in tumor tissue and effectively convert NIR light into local hyperthermia.

https://doi.org/10.1021/acsomega.2c02977
ACS Omega 2022, 7, 44643−44656

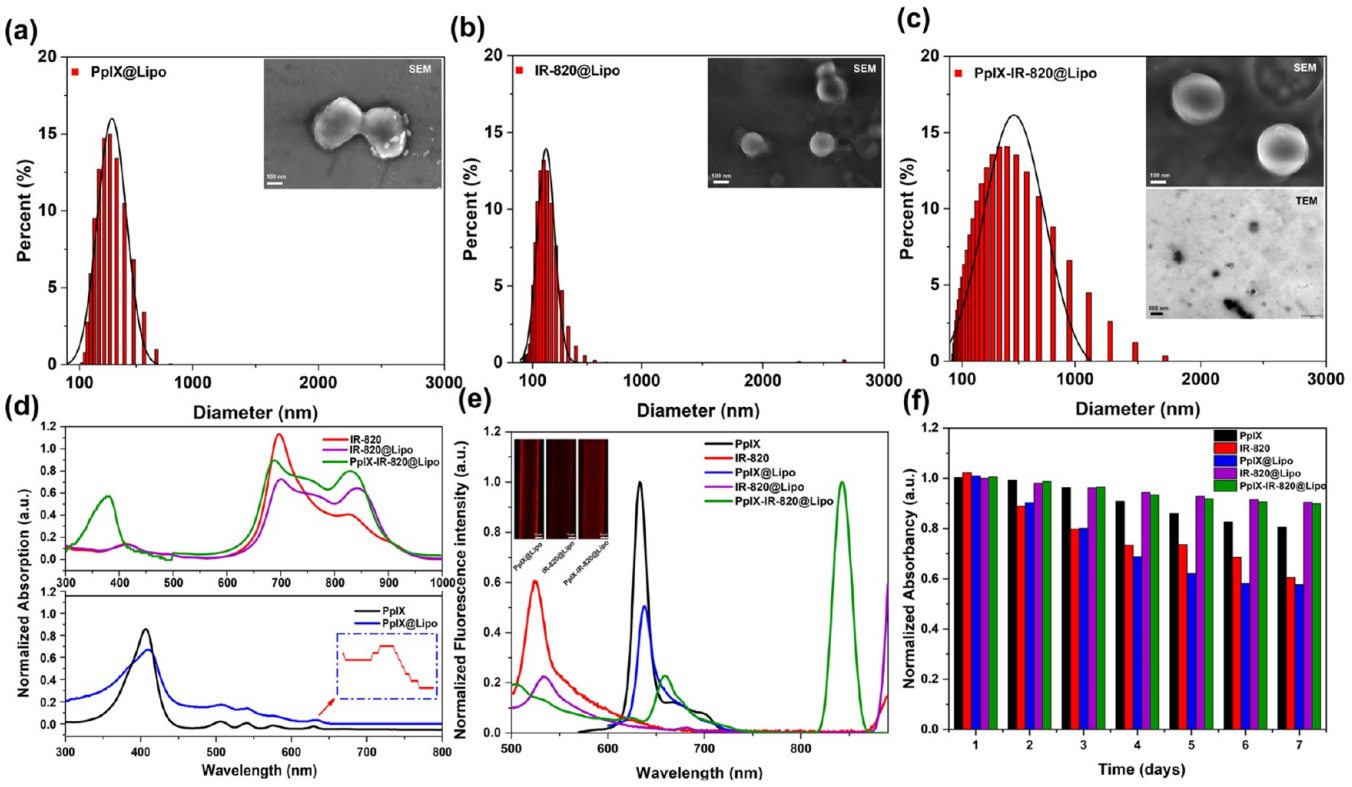

Figure 2. Hydrodynamic size distributions of (a) PpIX@Lipo NPs, (b) IR-820@Lipo NPs, and (c) PpIX-IR-820@Lipo NPs. Inset: SEM images (scale bar: 100 nm) and a TEM image (scale bar: 500 nm). (d) Absorption spectrum of PpIX-IR-820@Lipo NPs in aqueous dispersion. (e) Fluorescence spectrum of PpIX-IR-820@Lipo NPs in aqueous dispersion. Inset: PpIX@Lipo NPs, IR-820@Lipo NPs, and PpIX-IR-820@Lipo NPs in capillary glass tubes under confocal laser scanning microscopy (CLSM) (scale bar: 10 μm, λ_{ex} = 640 nm, λ_{em} = 800−1000 nm). (f) Absorption of PpIX-IR-820@Lipo NPs in aqueous dispersion for 7 days.

In addition, after liposome encapsulation, the water solubility and biocompatibility of theranostic nanoparticles could be enhanced greatly. Thus, liposomes have shown advantages in efficient multifunctional drug delivery.

In this work, a novel type of PDT/PTT theranostic nanoplatform was designed and synthesized. The PpIX (PS) and IR-820 (PTT agent) were encapsulated with liposomes to form PDT/PTT theranostic nanoplatform PpIX-IR-820@Lipo NPs. The PpIX-IR-820@Lipo NPs showed excellent water solubility and a spherical shape, with an average size of 380 nm, fluorescence peaks at 659 and 843 nm, and absorption peaks at 380 and 691 nm. Furthermore, PpIX-IR-820@Lipo NPs exhibited good cellular labeling ability and low cytotoxicity, without laser irradiation. Moreover, PpIX-IR-820@Lipo NPs showed an excellent PDT/PTT property on human cervical cancer cells (HeLa). High PDT/PTT synergistic efficiency could be obtained, with apoptosis of 70.5%. The novel PpIX-IR-820@Lipo NPs showed great potential in the treatment of cervical cancer.

2. RESULTS AND DISCUSSION

2.1. Synthesis and Characterization. PpIX is one of the popular PSs for its strong photosensitivity and efficiency. However, the poor water solubility of PpIX has hampered its further clinical application.[30,31] IR-820 is a derivative of ICG and shows strong NIR fluorescence and a photothermal effect. However, good biocompatibility is important for further biomedical research to retain the photothermal characteristics of IR-820.[32,33] Liposomes, as a drug delivery carrier, can encapsulate hydrophobic and hydrophilic drugs in the phospholipid bilayers and core.[34] Thus, liposomes may be an ideal carrier for the improvement of biocompatibility and water solubility of multifunctional theranostic nanoprobes.

The IR-820 and PpIX could be encapsulated well in the liposomes according to the preparation process shown in Figure 1 to form the PDT/PTT theranostic nanoplatform of PpIX-IR-820@Lipo NPs. The hydrophobic PpIX and liposomes formed a film after stirring with a magnetic stirrer. Then, hydrophilic IR-820 was sonicated to hydrate the formed film. After dialysis and filtration, PpIX-IR-820@Lipo NPs were obtained by the hydration film method.[35]

Then, the PpIX-IR-820@Lipo NPs and intermediate products (PpIX@Lipo NPs and IR-820@Lipo NPs) produced during the experiment were characterized. Transmission electron microscopy/scanning electron microscopy (SEM/TEM) and dynamic light scattering (DLS) characterizations were conducted on PpIX@Lipo NPs, IR-820@Lipo NPs, and PpIX-IR-820@Lipo NPs. These NPs displayed good spherical morphology and a relatively uniform particle size distribution, as shown in Figure 2a−c. The average size of the NPs was approximately 255.3 nm (PpIX@Lipo NPs), 195.4 nm (IR-820@Lipo NPs), and 380 nm (PpIX-IR-820@Lipo NPs). Among these, the PpIX-IR-820@Lipo NPs showed the largest particle size. The SEM and TEM images show that the PpIX-IR-820@Lipo NPs are uniformly spherical. As shown in Figure 2d, free PpIX and IR-820 exhibited two characteristic absorption peaks at 405 and 697 nm, respectively. After encapsulation, the absorption peaks of PpIX-IR-820@Lipo NPs shifted toward 380 and 691 nm. The slight shift of the absorption peak of PpIX-IR-820@Lipo NPs (green line) was

https://doi.org/10.1021/acsomega.2c02977
ACS Omega 2022, 7, 44643−44656

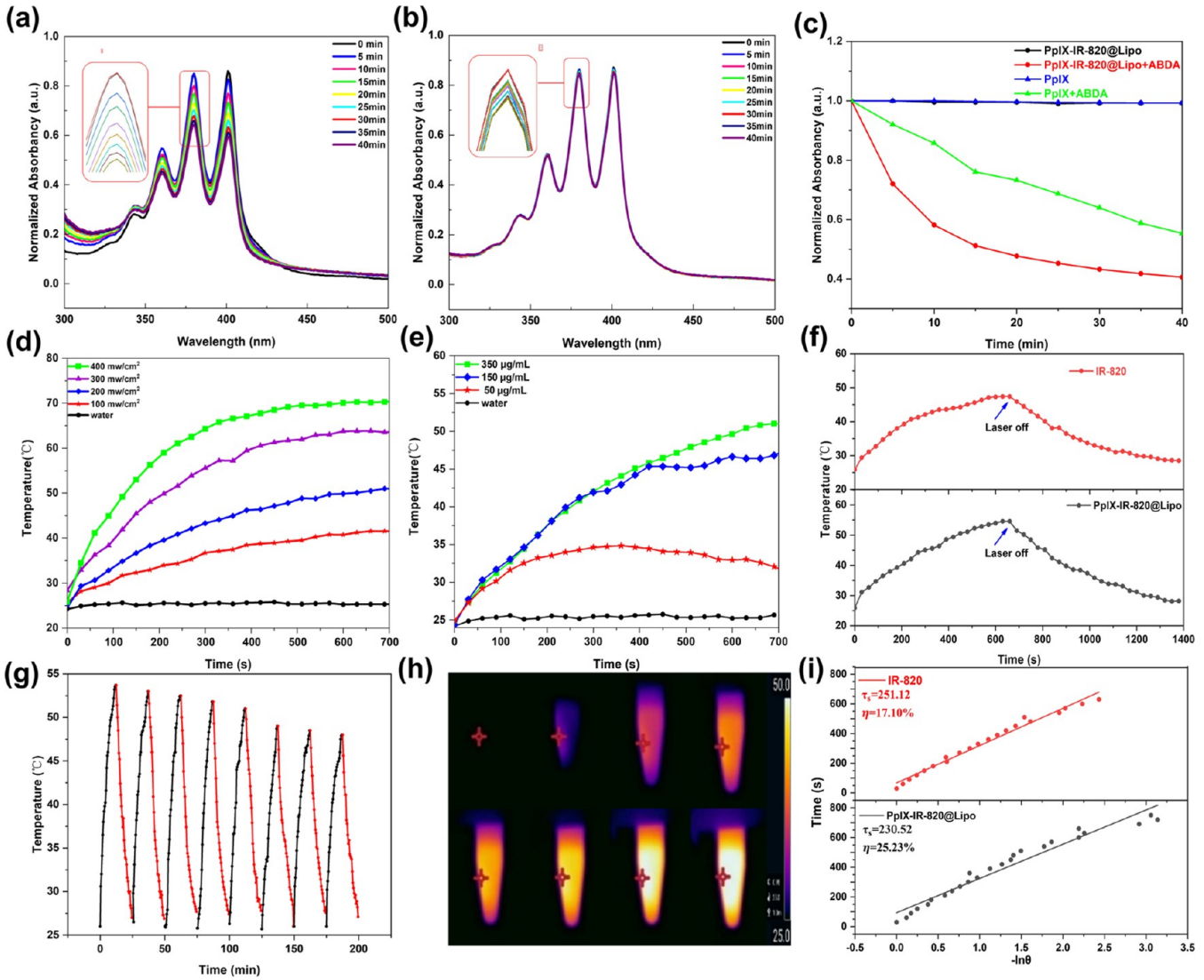

Figure 3. (a) Absorption peak intensities (at 375 nm) of ABDA and PpIX-IR-820@Lipo NPs mixture. (b) Absorption peak intensities (at 375 nm) of free PpIX-IR-820@Lipo NPs. (c) Decay curves of ABDA absorption at 375 nm in PpIX-IR-820@Lipo NPs or PpIX NPs dispersions after different durations of irradiation. (d) Photothermal heating curves of PpIX-IR-820@Lipo NPs (250 μg/mL) under 793 nm laser irradiation vs the irradiation time with varied power density. (e) Photothermal heating curves of PpIX-IR-820@Lipo NPs under 793 nm laser (200 mW/cm^2) irradiation vs the irradiation time with different concentrations. (f) Photothermal heating and (i) cooling curves and the heat transfer time constant calculated from the cooling time. (g) Heating curves of PpIX-IR-820@Lipo NPs for 8 laser ON/OFF cycles under irradiation with the 793 nm laser. (h) Photothermal heating images of PpIX-IR-820@Lipo NPs under 793 nm laser irradiations at different time intervals.

due to the conjugation of the molecule to the liposome,[36,37] further revealing that PpIX and IR-820 were successfully encapsulated. In addition, the concentration standard curve equation was obtained by fitting the concentration and absorption within a certain range according to the Lambert–Beer law.[38] The quantification of PpIX and IR-820 in PpIX-IR-820@Lipo NPs was confirmed. The drug loading content (DLC) and encapsulation efficiency (EE) of PpIX-IR-820@Lipo NPs were demonstrated by absorption spectroscopy.[39] The EE of PpIX and IR-820 was calculated as 92 and 27.11%, respectively, and the DLC of PpIX and IR-820 was determined to be 13.14 and 3.8%, respectively.

The fluorescence peaks of PpIX-IR-820@Lipo NPs were located at 659 and 843 nm (Figure 2e). Despite the peak drop, the characteristic peaks of free PpIX and IR-820 were maintained. Confocal laser scanning microscopy (CLSM) images of PpIX@Lipo NPs, IR-820@Lipo NPs, and PpIX-IR-820@Lipo NPs (200 μg/mL) in capillary glass tubes exhibited bright red fluorescence (Figure 2e inset). Furthermore, PpIX@Lipo NPs also exhibited red fluorescence under 366 nm light irradiation (Figure S1b). Fortunately, the fluorescence of PpIX-IR-820@Lipo NPs was not quenched and still had bright fluorescence. As shown in Figure 2f, the colloidal stability of the NPs was determined by measuring the absorption peaks for 7 consecutive days. PpIX-IR-820@Lipo NPs exhibited the best colloidal stability. The ζ potential of PpIX-IR-820@Lipo NPs (Figure S2a) showed a positive change in potential after coating. The changes in the absorption peaks of PpIX-IR-820@Lipo NPs after irradiation (405 and 691 nm) were measured (Figure S2b). The results show that after laser irradiation, the absorption peaks decreased and material degradation occurred.

2.2. ROS and Photothermal Analysis of PpIX-IR-820@Lipo NPs. The detection of ROS was under the irradiation of

https://doi.org/10.1021/acsomega.2c02977
ACS Omega 2022, 7, 44643−44656

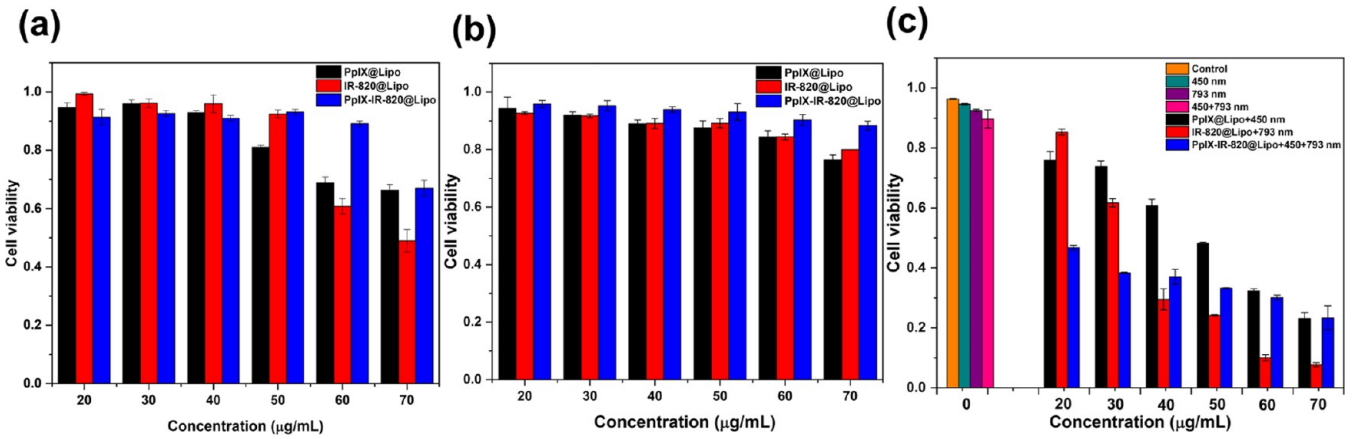

Figure 4. Cell viability analysis of (a) HeLa cells incubated in the dark, (b) H8 cells incubated in the dark, and (c) HeLa cells incubated with laser.

450 nm (1 W/cm^2) laser. Then, 1 mg/mL of 9,10-anthracenediyl-bis(methylene)dimalonic acid (ABDA) (60 μL) was added to the aqueous dispersion of PpIX-IR-820@Lipo NPs. ROS generation could be indirectly characterized by monitoring the absorption of ABDA at 375 nm. As shown in Figure 3a, the absorption of PpIX-IR-820@Lipo NPs was decreased significantly with increasing irradiation time. To confirm that the decrease in uptake was indeed due to the generation of ROS, the PpIX-IR-820@Lipo NPs group without laser irradiation was used for comparison (Figure 3b). The results show little change in absorption at 375 nm. In addition, the absorption of PpIX-IR-820@Lipo NPs was decreased greatly (Figures 3c and S3). These control experiments revealed that the reduced absorption at 375 nm was due to the copresence of PpIX-IR-820@Lipo NPs and ABDA. Under 450 nm irradiation, PpIX-IR-820@Lipo NPs could efficiently generate ROS.

The thermal effect of PpIX-IR-820@Lipo NPs in aqueous dispersion under 793 nm laser irradiation was explored. The temperature changes of PpIX-IR-820@Lipo NPs after irradiation were determined. Figure 3d shows the photothermal temperature curves of PpIX-IR-820@Lipo NPs under laser irradiation at different power densities (100, 200, 300, and 400 mW/cm^2). It was found that the temperature of PpIX-IR-820@Lipo NPs increased with power density under laser irradiation. IR-820 and IR-820@Lipo NPs exhibited the same characteristics upon laser irradiation (Figure S4). The photothermal temperature curves at different concentrations of PpIX-IR-820@Lipo NPs (50, 150, and 350 μg/mL) under laser irradiation are shown in Figure 3e. The temperature increased with increasing concentration. The results show that temperature was proportional to the concentration and power density. Note that within 8 min of irradiation, the solution temperature would reach 51.1 °C.

The photothermal stability of the infrared spectra of PpIX-IR-820@Lipo NPs was evaluated by thermal cycling. As shown in Figure 3g, under laser irradiation, there was little difference in the temperature change of PpIX-IR-820@Lipo NPs for 8 cycles of heating/cooling variation. IR-820 and IR-820@Lipo NPs also showed good stability (Figure S5). Note that as shown in Figures 3h and S6, no apparent thermal attenuation was observed even after the repeated cycling experiments, and PpIX-IR-820@Lipo NPs exhibited good photothermal properties. We calculated the photothermal conversion efficiency according to the formula 3. The η value of PpIX-IR-820@Lipo NPs was measured and calculated to be 25.23%, and the η value of IR-820 was 17.10% (Figure 3f,i). The η values of PpIX-IR-820@Lipo NPs were comparable to other IR-820-encapsulated polymer nanoparticles, such as IR-820@F-127 (35.2%)[40] and IR-820@PSMA (29.6%).[25] This indicates that PpIX-IR-820@Lipo NPs have good thermal conversion and stability and are expected to be reasonable PS candidates for PTT.

2.3. Cell Viability Analysis of PpIX-IR-820@Lipo NPs. The cell viability of PpIX@Lipo NPs, IR-820@Lipo NPs, and PpIX-IR-820@Lipo NPs was determined by the CCK-8 assay. We calculated the cell viability of HeLa cells and H8 cells incubated with PpIX@Lipo NPs, IR-820@Lipo NPs, and PpIX-IR-820@Lipo NPs. As shown in Figure 4a,b, PpIX-IR-820@Lipo NPs at concentrations ranging from 20 to 60 μg/mL were respectively incubated with HeLa/H8 cells for 6−8 h. It was clearly observed that at the concentration of 60 μg/mL, the group of PpIX-IR-820@Lipo NPs incubated with HeLa cells showed a cell viability of 89.13%, and the cell viability of the incubation group with H8 cells was 84.36%. The cell viability of PpIX@Lipo NPs incubated with HeLa cells was 68.83%, and that of H8 cells was 90.31%. Correspondingly, the cell viability of IR-820@Lipo NPs incubated with HeLa cells was 60.70%, and that of H8 cells was 84.39%. This result reveals that PpIX-IR-820@Lipo NPs possessed lower cell toxicity and good biocompatibility. Therefore, 50 μg/mL was selected for subsequent PDT/PTT studies. Furthermore, as shown in Figure 4c, PpIX-IR-820@Lipo NPs exhibited strong phototoxicity in HeLa cells upon laser irradiation. However, for the cells irradiated by laser only, the viability was >80%. The group of PpIX-IR-820@Lipo NPs + laser at a concentration of 30 μg/mL showed a high phototoxicity of 38.30%. In addition, the PpIX@Lipo NPs showed a cell viability of 73.88%, and IR-820@Lipo NPs showed a cell viability of 61.71%. Therefore, the liposome-encapsulated PpIX-IR-820@Lipo NPs exhibited low cytotoxicity and good phototoxicity, which improved the biocompatibility of PpIX-IR-820@Lipo NPs.

2.4. Near-Infrared Fluorescence Cell Imaging Analysis of PpIX-IR-820@Lipo NPs. The cellular labeling ability of PpIX@Lipo NPs (25 μg/mL), IR-820@Lipo NPs, and PpIX-IR-820@Lipo NPs at the IR-820 concentration of 50 μg/mL was analyzed and presented. HeLa cells were treated with NPs for 2 h. The blue channel (λ_{ex} = 488 nm) represents the existence of Hoechst 33342. The red channel (λ_{ex} = 640 nm)

https://doi.org/10.1021/acsomega.2c02977
ACS Omega 2022, 7, 44643−44656

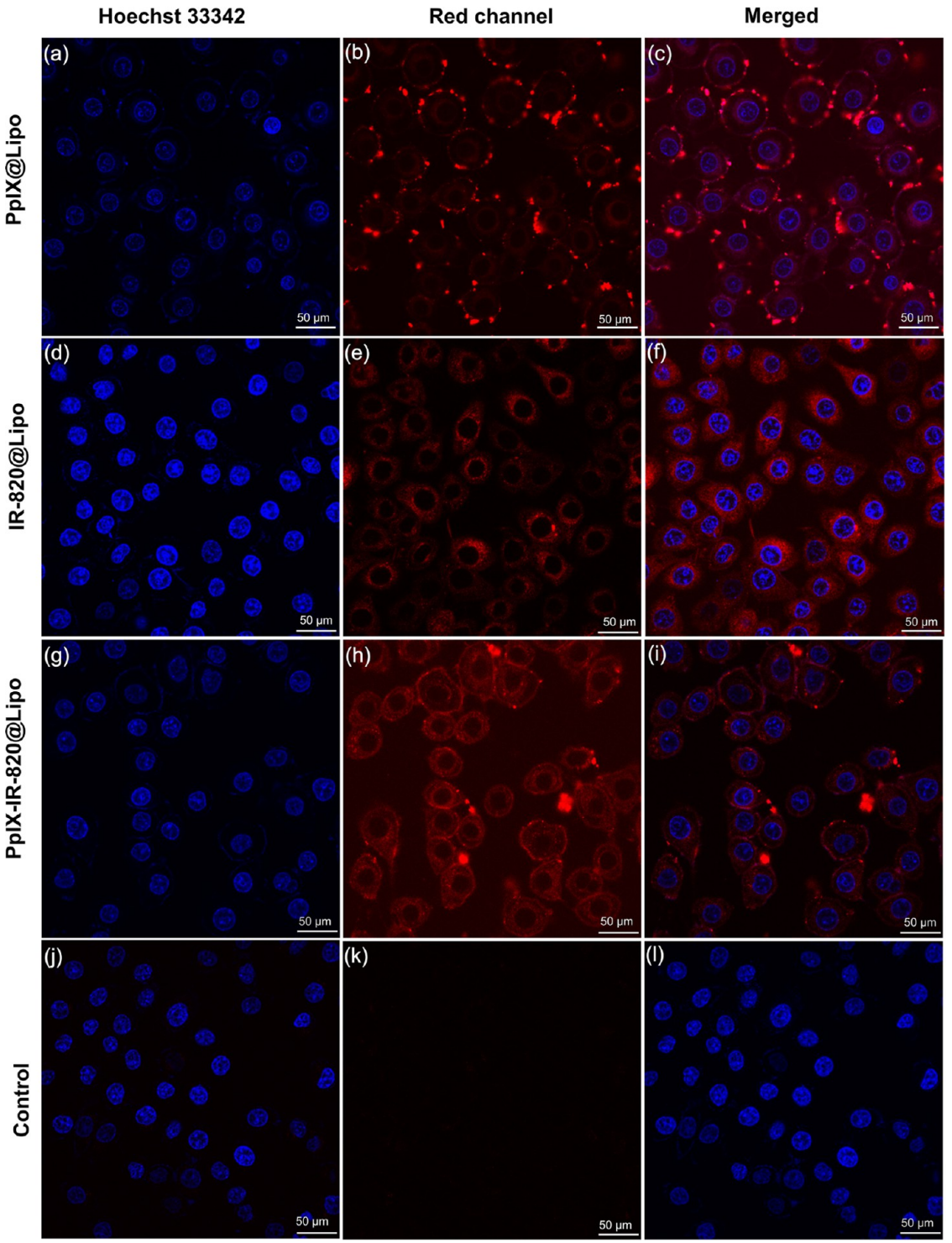

Figure 5. (a–c) PpIX@Lipo NPs, (d–f) IR-820@Lipo NPs, (g–i) PpIX-IR-820@Lipo NPs, and (j–l) HeLa cells without incubation of NPs under CLSM are labeled (scale bar: 50 μm, λ_{ex} = 640 nm, λ_{em} = 800−1000 nm).

represents the fluorescence of PpIX and IR-820. Hoechst 33342 and PpIX/IR-820 channels were merged to confirm cellular uptake. Both images were collected from fluorescence from NPs in cells under a 60× objective lens (scale bar: 50 μm, λ_{ex} = 640 nm, λ_{em} = 800−1000 nm).

As shown in Figure 5, PpIX@Lipo NPs, IR-820@Lipo NPs, and PpIX-IR-820@Lipo NPs had good cellular uptake. The accumulation of NPs on cells formed the speckled fluorescent bright spots. PpIX@Lipo NPs aggregated on the cell membrane, and IR-820@Lipo NPs aggregated in the cell cytoplasm. PpIX-IR-820@Lipo NPs aggregated in the cell membrane and cytoplasm, which exhibited fluorescence signals in the red channel. PpIX-IR-820@Lipo NPs enhanced the fluorescence intensity in the cell membrane and cytoplasm. We also investigated the cellular uptake of free PpIX (Figure S7a–c) and IR-820 (Figure S7d–f). Free PpIX and IR-820 were efficiently taken up by cells and fluoresced brightly in the red

https://doi.org/10.1021/acsomega.2c02977
ACS Omega 2022, 7, 44643−44656

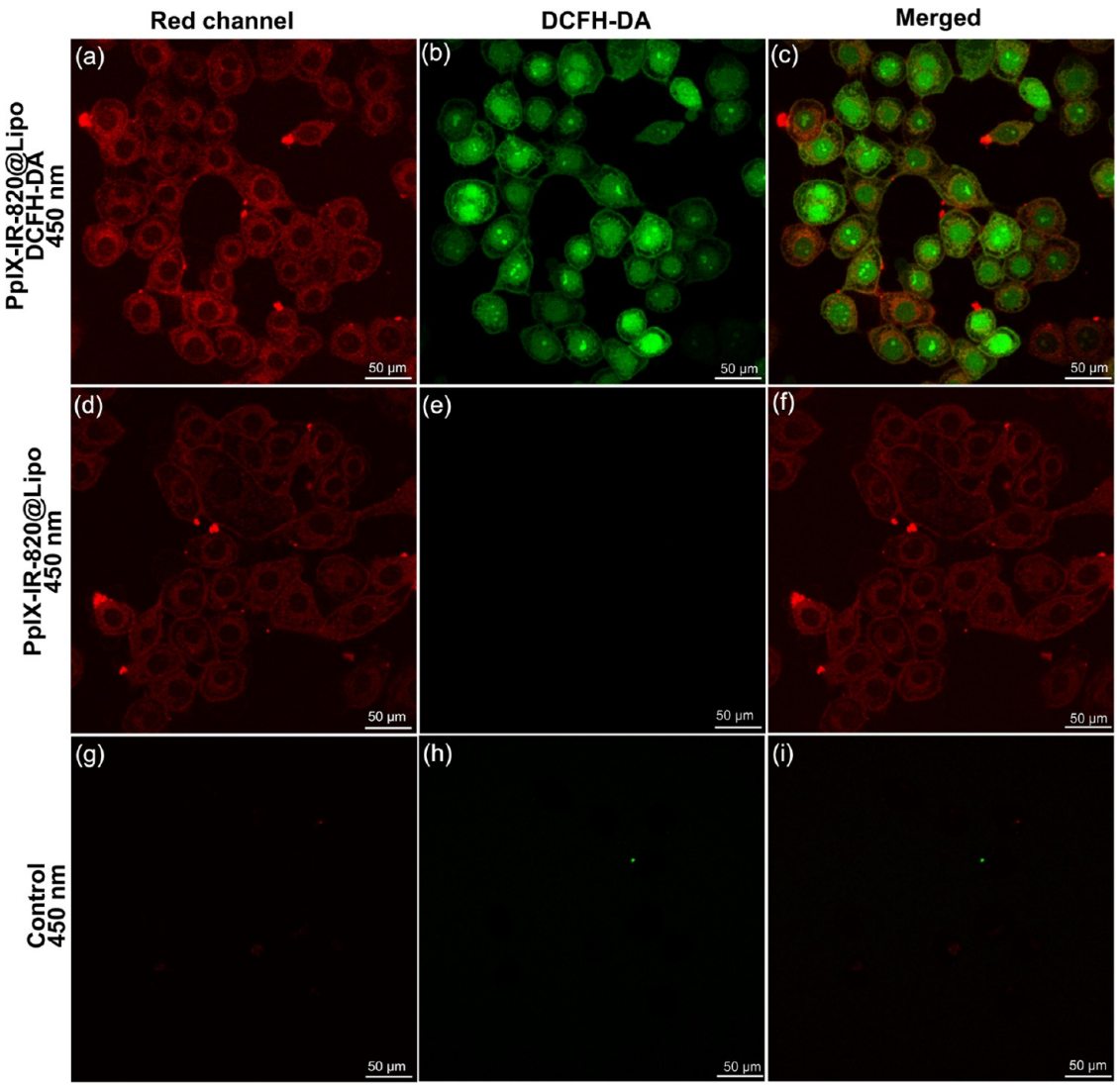

Figure 6. Intracellular ROS evaluation of PpIX-IR-820@Lipo NPs on HeLa cells. (a, d, g) CLSM fluorescence images of PpIX-IR-820@Lipo NPs-treated HeLa cells in the red channel. (b, e, h) CLSM fluorescence images of PpIX-IR-820@Lipo NPs-treated HeLa cells by DCFH-DA in the green channel. (c, f, i) Overlap of red and green channels (scale bar: 50 μm, λ_{ex} = 640 nm, λ_{em} = 800−1000 nm).

channel, but free PpIX was poorly morphologically cultured with cells.

2.5. Intracellular ROS and PDT/PTT Analysis. The ROS generation efficiency of PpIX-IR-820@Lipo NPs in HeLa cells was evaluated. ROS can oxidize nonfluorescent DCFH-DA to generate fluorescent DCF using 488 nm light excitation, which produces green fluorescence with an intensity proportional to the ROS level.[41] Therefore, DCFH-DA was chosen as an indicator of ROS production. HeLa cells were treated with NPs for 2 h. The green channel (λ_{ex} = 488 nm) represents the existence of DCF. The red channel (λ_{ex} = 640 nm) represents the fluorescence of PpIX. Both are images of NPs fluorescent cells under a 60× objective lens (scale bar: 50 μm, λ_{ex} = 640 nm, λ_{em} = 800−1000 nm).

As shown in Figure 6a−c, PpIX-IR-820@Lipo NPs were first incubated with HeLa cells and irradiated with 450 nm 1 W/cm^2 laser (5 min). With the help of DCFH-DA, a strong fluorescence signal in the green channel was observed in the cells, accounting for 95.24%. It was shown that a large amount of ROS was generated, resulting in the death of HeLa cells. In contrast, as shown in Figure 6d−f, only the PpIX-IR-820@Lipo NPs group exhibited no fluorescence in the cells, and there was red fluorescence. As shown in Figure 6g−i, only the DCFH-DA group did not show any fluorescence in the cells. In addition, we also assayed ROS production by free PpIX (Figure S8a−f) and PpIX@Lipo NPs (Figure S8g−l). These results reveal that the intracellular PpIX-IR-820@Lipo NPs would generate ROS after laser irradiation, resulting in a PDT effect.

The apoptosis analysis of PDT/PTT of PpIX-IR-820@Lipo NPs was performed. HeLa cells were incubated with PpIX-IR-820@Lipo NPs and annexin V-fluorescein isothiocyanate (FITC). Then, 793 and 450 nm (1 W/cm^2) lasers were utilized for irradiation for 5 min. Annexin V-FITC can bind to apoptotic cell membranes expressing phosphatidylserine and emit green fluorescence under excitation at 488 nm.[42] The green channel (λ_{ex} = 488 nm) represents the fluorescence of FITC-bound apoptotic cell proteins. The red channel (λ_{ex} = 640 nm) represents the fluorescence of IR-820. Both are images of NPs fluorescent cells under a 60× objective lens (scale bar: 50 μm, λ_{ex} = 640 nm, λ_{em} = 800−1000 nm).

https://doi.org/10.1021/acsomega.2c02977
ACS Omega 2022, 7, 44643−44656

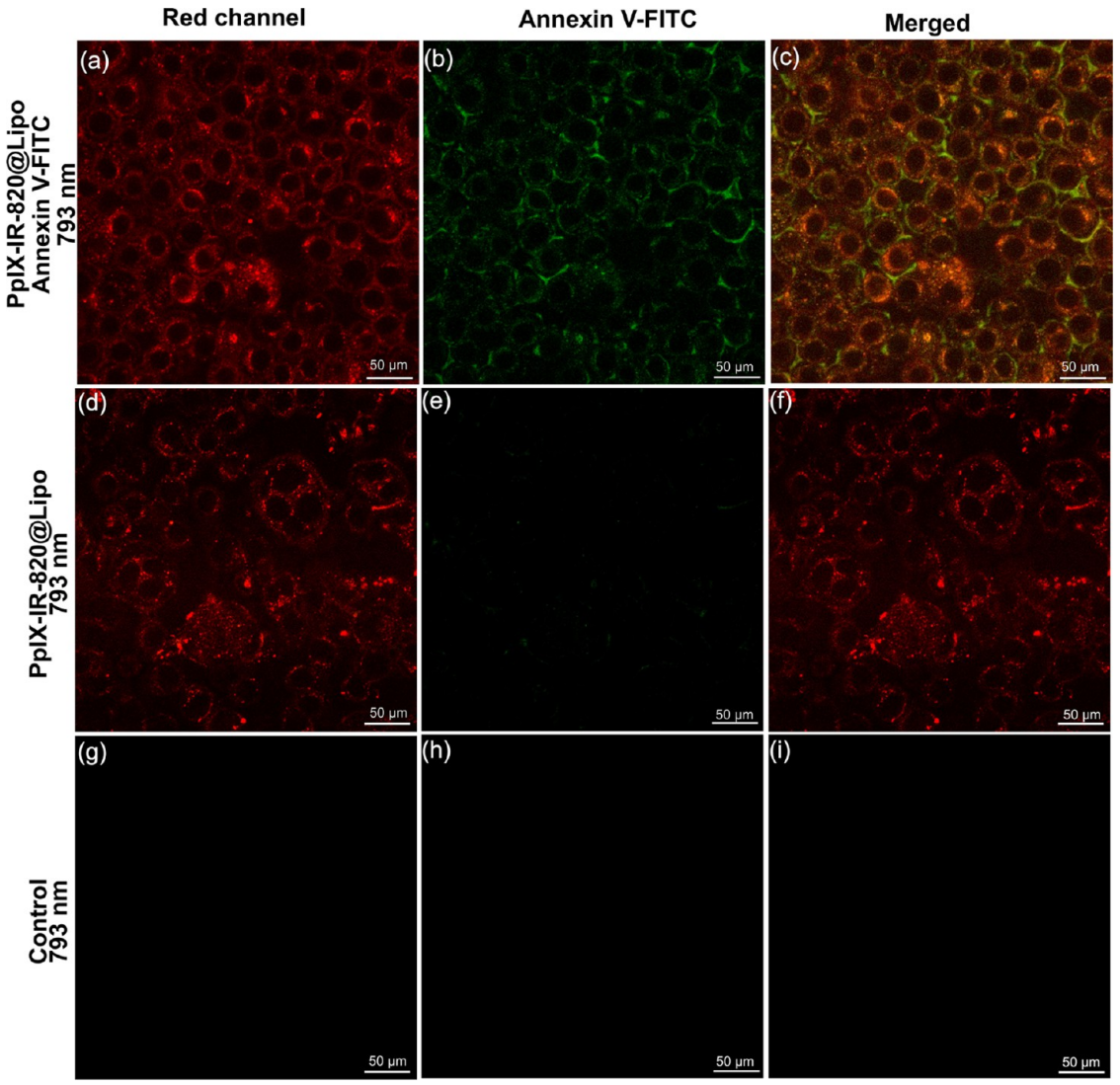

Figure 7. Apoptosis rate evaluation of PpIX-IR-820@Lipo NPs under 793 nm laser irradiation on HeLa cells. (a, d, g) CLSM fluorescence images of PpIX-IR-820@Lipo NPs-treated HeLa cells in the red channel. (b, e, h) CLSM fluorescence images of PpIX-IR-820@Lipo NPs-treated HeLa cells by annexin V-FITC in the green channel. (c, f, i) Overlap of red and green channels (scale bar: 50 μm, λ_{ex} = 640 nm, λ_{em} = 800−1000 nm).

As shown in Figure 7a−c, a strong fluorescence signal in the green channel was observed in most cells after irradiation. This result reveals that PpIX-IR-820@Lipo NPs had the potential to heat up, leading to the apoptosis process of HeLa cells. In both control experiments, no fluorescence was observed (Figure 7d−i). In addition, we determined the apoptosis of free IR-820 (Figure S9a−f) and IR-820@Lipo NPs (Figure S9g−l). These results indicate that the intracellular PpIX-IR-820@Lipo NPs need to convert heat under the combined action of a laser and have a great PTT effect.

As shown in Figure 8a−c, the strong fluorescence signal in the green channel was observed in most cells treated with NPs after irradiation. This result reveals that PpIX-IR-820@Lipo NPs could generate ROS, which could lead to the apoptosis of HeLa cells. In both control experiments, no fluorescence signal could be observed in the green channel (Figure 8d−i). In addition, we also determined the apoptosis of free PpIX (Figure S10a−f) and PpIX@Lipo NPs (Figure S10g−l). These results indicate the efficient intracellular PDT property of PpIX-IR-820@Lipo NPs under 450 nm laser irradiation.

2.6. PDT/PTT Synergistic Analysis in Living Cells. PDT and PTT can induce cell death through apoptosis, necrosis, and autophagy pathways.[43] The lower left quadrant of flow cytometry images is the live cell population, the lower right quadrant is the early apoptotic (annexin V-FITC positive) population, the upper left quadrant is the necrotic cell (annexin V-FTIC negative) population, and the upper right is the late apoptotic population.[44] The flow cytometry (annexin V-FITC/PI staining method) was utilized to quantitatively verify whether NPs-mediated PDT/PTT can induce cell apoptosis. The PpIX@Lipo NPs were irradiated with a 450 nm laser to activate PDT. PTT was activated by irradiating IR-820@Lipo NPs with a 793 nm laser. PDT/PTT was activated by coirradiating PpIX-IR-820@Lipo NPs with 450 and 793 nm lasers.

As shown in Figure 9a,c,e, compared with the control group (Figure 9g), laser irradiation had no effect on cells. As shown in Figure 9b, the apoptosis and necrosis in the PpIX@Lipo NPs laser group were higher than those in the laser group (Figure 9a), but the number of cells in the PpIX@Lipo NPs laser group was less in the presence of the same experimental

https://doi.org/10.1021/acsomega.2c02977
ACS Omega 2022, 7, 44643−44656

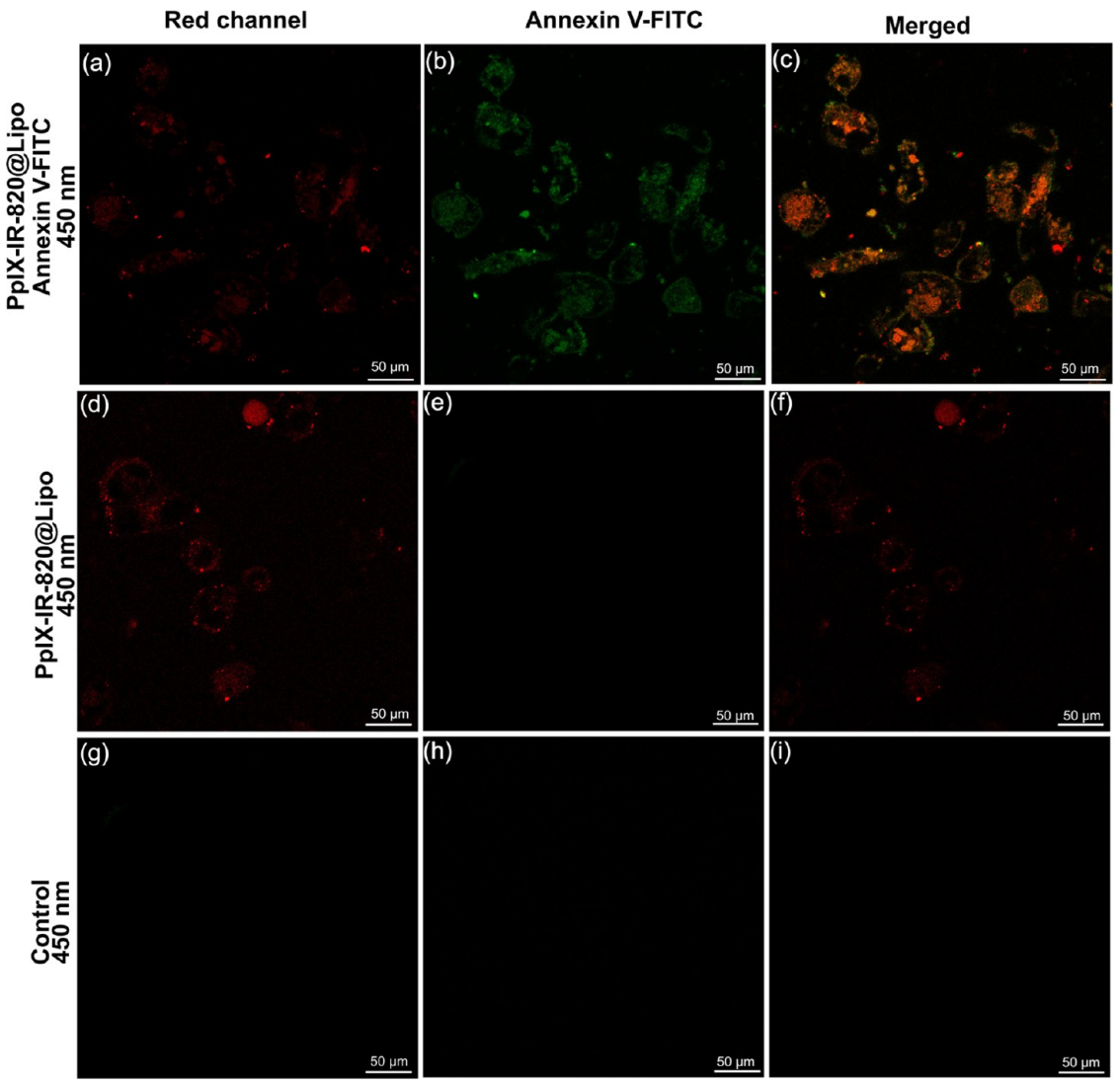

Figure 8. Apoptosis rate evaluation of PpIX-IR-820@Lipo NPs by 450 nm laser irradiation on HeLa cells. (a, d, g) CLSM fluorescence images of PpIX-IR-820@Lipo NPs-treated HeLa cells in the red channel. (b, e, h) CLSM fluorescence images of PpIX-IR-820@Lipo NPs-treated HeLa cells by annexin V-FITC in the green channel. (c, f, i) Overlap of red and green channels (scale bar: 50 μm, λ_{ex} = 640 nm, λ_{em} = 800−1000 nm).

conditions, which may have resulted from the potential toxicity of PpIX@Lipo NPs. As shown in Figure 9d, the apoptosis of cells in the IR-820@Lipo NPs laser group was higher than that in the laser group (Figure 9c). As shown in Figure 9f, the apoptosis of PpIX-IR-820@Lipo NPs laser group was higher than that of the laser group (Figure 9e). Therefore, we conclude that nanoparticle-mediated PDT and PTT induce apoptosis in cancer cells. Notably, cells treated with PpIX-IR-820@Lipo NPs underwent more apoptosis after laser irradiation, revealing that PDT/PTT had a significant effect.

3. CONCLUSIONS

In conclusion, the combined therapy of PDT/PTT not only overcomes the shortcomings of traditional cervical cancer treatment but also greatly enhances the therapeutic effect. The novel PpIX-IR-820@Lipo NPs were designed and synthesized by a simple and reproducible hydration film method. PpIX-IR-820@Lipo NPs exhibited good water solubility and stability. After encapsulation, the PpIX-IR-820@Lipo NPs generated ROS, and the photothermal conversion efficiency could reach 25.23%. Furthermore, PpIX-IR-820@Lipo NPs showed low cytotoxicity in HeLa cells, and excellent fluorescent labeling ability was confirmed. In addition, the PDT/PTT efficiency of PpIX-IR-820@Lipo NPs on HeLa cells was verified to be high (70.5%). The results indicate that PpIX-IR-820@Lipo NPs can act as photosensitizers to enhance the synergistic therapy of PDT and PTT, which can provide a new direction for the treatment of cervical cancer.

4. EXPERIMENTAL METHODS

4.1. Materials and Methods. Cholesterol (Chol), L-α-phosphatidylcholine (L-α-lecithin), and 2′-(4-ethoxyphenyl)-5-(4-methyl-1-piperazinyl)-2,5′-bi-1*H*-benzimidazole (Hoechst 33342) were purchased from Beijing Solarbio Science & Technology Co., Ltd. (China). Tetrahydrofuran (THF), chloroform, PpIX, IR-820, 9,10-anthracenediyl-bis-(methylene)dimalonic acid (ABDA), and 2′,7′-dichlorofluorescin diacetate (DCFH-DA) were purchased from Shanghai Aladdin Biochemical Technology Co., Ltd. (China). 2-(2-Methoxy-4-nitrophenyl)-3-(4-nitrophenyl)-5-(2,4-disulfophenyl)-2*H*-tetrazolium sodium salt (CCK-8 assay) was purchased from Beijing Bioss Biotechnology Co., Ltd. (China). Dimethyl

https://doi.org/10.1021/acsomega.2c02977
ACS Omega 2022, 7, 44643−44656

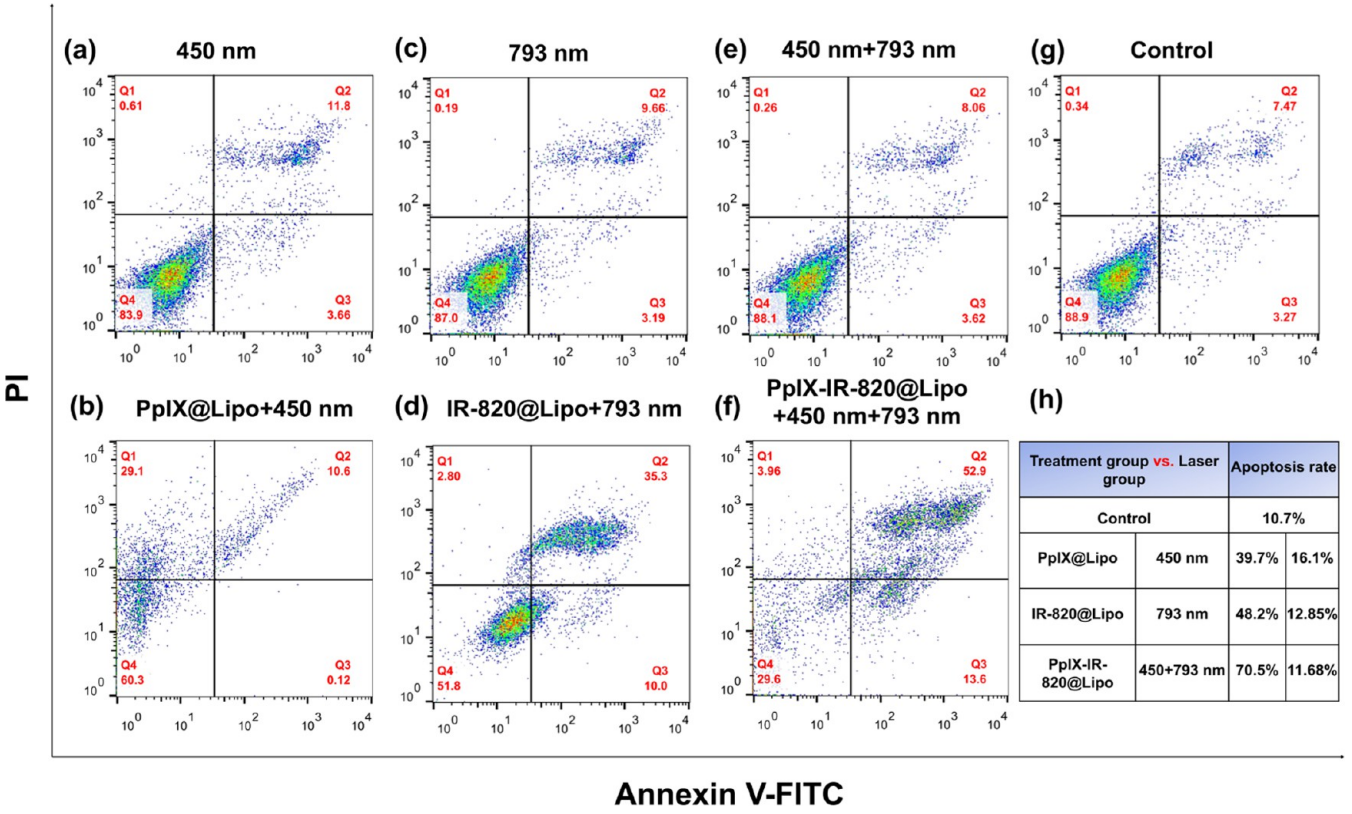

(h)

Treatment group vs. Laser group		Apoptosis rate	
Control		10.7%	
PpIX@Lipo	450 nm	39.7%	16.1%
IR-820@Lipo	793 nm	48.2%	12.85%
PpIX-IR-820@Lipo	450+793 nm	70.5%	11.68%

Figure 9. Apoptosis of HeLa cells induced by PpIX-IR-820@Lipo NPs-mediated PDT/PTT. Representative dot plots of annexin V-FITC stained cells: (a) 450 nm, (b) PpIX@Lipo NPs irradiated with a 450 nm laser, (c) 793 nm, (d) IR-820@Lipo NPs with 793 nm laser irradiation, (e) 450 and 793 nm, (f) PpIX-IR-820@Lipo NPs coirradiated with 450 and 793 nm lasers (1 W/cm^2 for 5 min), and (g) control. (h) Comparison table of apoptosis rates of NPs treatments on HeLa cells.

sulfoxide (DMSO), Dulbecco's modified Eagle's medium (DMEM), trypsin, and phosphate-buffered saline (PBS) were purchased from Shanghai Hyclone Co., Ltd. (China). Fetal bovine serum (FBS) was purchased from GIBCO (Australia). An annexin V-FITC apoptosis detection kit was purchased from BD Co., Ltd. Deionized water (DIW) was used in all experimental processes.

The PpIX-IR-820@Lipo NPs were examined by a transmission electron microscope (TEM, JEM-1230, JEOL, Ltd., Japan) operated in bright-field mode for morphological evaluation. The microstructure was characterized by scanning electron microscopy (SEM, JSM-7610FPlus, Japan, operated at 5 kV). The size of the PpIX-IR-820@Lipo NPs was characterized with the DLS method at 25 °C using a Zetasizer Nano ZS-90 (Malvern, U.K.). Absorption spectra were recorded on a Shimadzu UV-2700 spectrophotometer (Japan). Fluorescence spectra were recorded on a Shimadzu RF-5301 PC spectrophotometer (a xenon lamp and monochromator were used for excitation, and the emission band was 220−900 nm, Japan). A CLSM (NIKON C2$^+$, Japan) was utilized for the NIR fluorescence microscopic imaging. An FACSCalibur flow cytometer (BD LSR II) was used to quantify the PDT/PTT efficiency of the PpIX-IR-820@Lipo NPs on HeLa cells.

4.2. Synthesis of PpIX-IR-820@Lipo NPs. PpIX- and IR-820-loaded liposomes (PpIX-IR-820@Lipo) were prepared using the hydration film method.[45−47] The L-α-lecithin, cholesterol, PpIX, and IR-820 NPs were prepared at the weight ratio of 4:1:1:1. L-α-Lecithin and cholesterol were dissolved in chloroform. PpIX was dissolved in tetrahydrofuran (THF), and IR-820 was dissolved in DIW. L-α-Lecithin, cholesterol, and PpIX were first evaporated using a magnetic stirrer until a lipid film formed. Subsequently, IR-820 solution and PBS were added for hydration at 40 °C and then sonicated with an ultrasonic cleaner for 15 min. The liposome suspension was dialyzed through a dialysis bag with a molecular weight of 3000 Da and then filtered four to five times to obtain PpIX-IR-820@Lipo NPs, which were stored in a refrigerator at 4 °C in the dark until further use. PpIX@Lipo NPs and IR-820@Lipo NPs were prepared in the same way.

4.3. Characterization of PpIX-IR-820@Lipo NPs. The particle size and ζ potential distributions of PpIX@Lipo NPs, IR-820@Lipo NPs, and PpIX-IR-820@Lipo NPs were determined, respectively. The morphological features of the particles were observed by SEM and TEM. The absorption spectra of NPs in aqueous dispersion (5 μg/mL) and the colloidal stability for 7 days were recorded. The fluorescence spectra of NPs in aqueous dispersion (200 μg/mL) were measured. The measurement of PpIX and IR-820 in PpIX-IR-820@Lipo NPs was confirmed by the concentration standard curve assay.[48] To determine drug loading content (DLC) and encapsulation efficiency (EE), supernatants from three centrifugation cycles were collected when preparing PpIX@Lipo NPs, IR-820@Lipo NPs, and PpIX-IR-820@Lipo NPs. The absorption spectra of the supernatants were collected after each washing step and further measured. The contents of PpIX and IR-820 in the supernatant were determined from the corresponding standard curves at 405 and 691 nm, respectively. The DLC and EE were calculated according to eqs 1 and 2:

https://doi.org/10.1021/acsomega.2c02977
ACS Omega 2022, 7, 44643−44656

$$\text{DLC}\ (\%) = \frac{W_{\text{PpIX/820}} - W_{\text{Drug in supernatant}}}{W_{\text{PpIX-IR-820@Lipo}}} \times 100\% \quad (1)$$

$$\text{EE}\ (\%) = \frac{W_{\text{PpIX/820}} - W_{\text{Drug in supernatant}}}{W_{\text{T}}} \times 100\% \quad (2)$$

where $W_{\text{PpIX/820}}$ is the quantity of PpIX or IR-820 in the PpIX-IR-820@Lipo NPs, $W_{\text{PpIX-IR-820@Lipo}}$ is the weight of the PpIX-IR-820@Lipo NPs, and W_{T} is the total weight of the PpIX or IR-820 added.[49,50] The NIR fluorescence of NPs was explored. PpIX@Lipo NPs, IR-820@Lipo NPs, and PpIX-IR-820@Lipo NPs in aqueous dispersion (200 μg/mL) were absorbed by capillaries and placed under a CLSM. The fluorescence intensity of continuous illumination at 640 nm under a 10× objective lens was recorded.

4.4. Singlet Oxygen Generation Measurements. The chemical reaction of ABDA with PpIX, PpIX@Lipo NPs, and PpIX-IR-820@Lipo NPs can indirectly characterize the ROS generation efficiency.[51,52] ABDA was dissolved in DMSO (1 mg/mL), and 60 μL was added to the NPs aqueous dispersion. The dispersion was irradiated with a 450 nm 1 W/cm^2 laser, resulting in a decrease in the absorption of ABDA (375 nm), which was detected every 5 min for 40 min.

4.5. Photothermal Analysis. The photothermal effects of IR-820, IR-820@Lipo NPs, and PpIX-IR-820@Lipo NPs (250 μg/mL) were analyzed under the irradiation of a 793 nm laser at 4 power densities (50, 150, 250, and 350 mW/cm^2). The temperature changes were then recorded. In addition, 250 mW/cm^2 was analyzed under the irradiation of a 793 nm laser at 3 various concentrations (50, 150, and 350 μg/mL), and the temperature changes were observed. Then, 250 μg/mL was analyzed in a hot−cold cycle irradiated with a 793 nm laser (250 mW/cm^2) for 10 min, followed by natural cooling for 10 min, which was repeated for 8 cycles. The thermal images were recorded every 30 s with an infrared thermal imager (Fotri323Pro #L25) for 10 min.

The photothermal conversion efficiency (η) of PpIX-IR-820@Lipo NPs (IR-820 concentration: 250 μg/mL) was measured as follows: PpIX-IR-820@Lipo NPs were dispersed in DIW and irradiated under a 793 nm NIR laser (250 mW/cm^2, 12 min). The temperature curve when the laser was on and off was recorded, and η could be calculated by the following equation:[53,54]

$$\eta\ (\%) = \frac{M_{\text{D}}C_{\text{D}}(T_{\text{Max}} - T_{\text{Max,water}})}{\tau_{\text{s}}I(1 - 10^{-A_{793}})} \times 100\% \quad (3)$$

where T_{Max} and $T_{\text{Max,water}}$ represent the maximum equilibrium temperature for PpIX-IR-820@Lipo NPs solution and water, respectively. I is the NIR laser power density, and A_{793} is the absorption of dispersion at 793 nm, measured using the time constant τ_{s} of the system with the help of the mass (M_{D}) and the heat capacity (C_{D}) of DIW.

4.6. Cell Culture. HeLa cells and H8 cells were cultured in DMEM with 10% FBS, 1% penicillin, and 1% amphotericin B at 37 °C in a humidified incubator containing 5% CO_2. The cells were seeded in 60 mm cell culture dishes, and after reaching a high degree of confluence, they were collected with trypsin solution for subsequent experiments.

4.7. Cellular Uptake Experiment. In a 35 mm Petri dish, 2 × 10^5 cells were cultured and incubated for 24 h. Then, 50 μg/mL IR-820, IR-820@Lipo NPs, or PpIX-IR-820@Lipo NPs and 25 μg/mL PpIX or PpIX@Lipo NPs were added to the cells, incubated for 2 h, and washed three times with 1× PBS. Then, a new medium containing 1 mg/mL Hoechst 33342 was added for nucleus staining, and the cells were washed three times with 1× PBS. Finally, 600 μL of culture medium was added, and cells were imaged with a CLSM. The Hoechst 33342 channel signal overlapped with the PpIX (IR-820) channel signal.

4.8. Cellular Viability Study. Cell viability and dark toxicity of PpIX@Lipo NPs, IR-820@Lipo NPs, and PpIX-IR-820@Lipo NPs on HeLa and H8 cells were detected by CCK-8 assay. Furthermore, the phototoxicity of PpIX-IR-820@Lipo NPs to HeLa/H8 was studied. First, 5 × 10^3 cells/well were cultured in a 96-well plate for 24 h to complete cell attachment. Different concentrations of PpIX-IR-820@Lipo NPs were added and incubated for 6−8 h to allow for the cellular uptake of the PpIX-IR-820@Lipo NPs. After PpIX-IR-820@Lipo NPs were incubated with cells, 10 μL of CCK-8 detection solution was added to one well in dark conditions and incubated for 2−4 h. Phototoxicity detection was obtained under laser (450 and 793 nm, 1 W/cm^2) irradiation for 5 min after incubation. Optical density (OD) was then recorded at 450 nm, and all plates were covered with aluminum foil to protect them from light. Cell viability was determined by comparing the OD values of the treatment and control groups as follows:[55−57]

$$\text{cell viability}\ (\%) = \frac{\text{OD}_{\text{treatment}} - \text{OD}_{\text{blank}}}{\text{OD}_{\text{control}} - \text{OD}_{\text{blank}}} \times 100\% \quad (4)$$

where $\text{OD}_{\text{treatment}}$, $\text{OD}_{\text{control}}$, and OD_{blank} are the ODs recorded for the treatment, control, and blank groups, respectively. Each experiment was performed at least three times. Cell viabilities were expressed as the mean ± standard deviation.

4.9. Intracellular ROS Generation and PDT/PTT Detection. Intracellular ROS production of PpIX@Lipo NPs and PpIX-IR-820@Lipo NPs was detected with DCFH-DA. The apoptosis rate of cells stimulated by IR-820@Lipo NPs and PpIX-IR-820@Lipo NPs under 793 nm laser irradiation was detected by annexin V-FITC. The apoptosis rate of cells stimulated by PpIX@Lipo NPs and PpIX-IR-820@Lipo NPs under 450 nm laser irradiation was detected by annexin V-FITC. First, 2 × 10^5 cells were incubated in 35 mm dishes for 24 h at 37 °C, 5% CO_2. Cells were used to adhere to and remove the culture medium, and then, the cell plate was washed twice with PBS buffer. After incubation with NPs (concentration consistent with 2.9) in the dark for 2 h, DCFH-DA and annexin V-FITC probes were loaded for 30 and 10 min and then washed twice with PBS. Then, a fresh culture medium was added. The DCFH-DA/annexin V-FITC group was irradiated at 450/793 nm (1 W/cm^2) for 5 min. Finally, the fluorescence images of cells were obtained by CLSM. The red fluorescence from NPs and the green fluorescence of DCFH-DA/annexin V-FITC were simultaneously observed.

4.10. In Vitro PDT/PTT Analysis. The quantitative apoptosis of PDT, PTT, and PDT/PTT under the combined effect of NPs and the laser was explored. HeLa cells were seeded in 6-well plates at 1 × 10^5 cells per well and incubated overnight. PpIX@Lipo NPs, IR-820@Lipo NPs, and PpIX-IR-820@Lipo NPs were subsequently incubated in the dark for 2 h. PpIX@Lipo NPs were irradiated with a 450 nm laser. IR-820@Lipo NPs were irradiated with a 793 nm laser. PpIX-IR-820@Lipo NPs were irradiated with a 450 and 793 nm dual-laser continuous laser. The power was 1 W/cm^2, and the

https://doi.org/10.1021/acsomega.2c02977
ACS Omega 2022, 7, 44643−44656

irradiation time was 5 min/hole. They were then incubated with annexin V-FITC/PI for 10 min in the dark and quantitatively assessed using a flow cytometer (BD LSR II).

■ ASSOCIATED CONTENT

Supporting Information

The Supporting Information is available free of charge at https://pubs.acs.org/doi/10.1021/acsomega.2c02977.

Images of IR-820@Lipo NPs, PpIX@Lipo NPs, and PpIX-IR-820@Lipo NPs under day light and 366 nm light, respectively; absorption peak intensities of PpIX-IR-820@Lipo NPs before and after laser irradiation; photothermal heating curves of free IR-820 and IR-820@Lipo NPs under laser irradiation; heating curves of IR-820 and IR-820@Lipo NPs for 8 laser ON/OFF cycles under laser irradiation; photothermal heating images of IR-820 and IR-820@Lipo NPs under laser irradiations at different time intervals; free PpIX and IR-820 NPs in HeLa cells under a CLSM; intracellular ROS evaluation of free PpIX and PpIX@Lipo NPs on HeLa cells; and apoptosis rate evaluation of free IR-820, IR-820@Lipo, PpIX, and PpIX@Lipo NPs on HeLa cells (PDF)

■ AUTHOR INFORMATION

Corresponding Authors

Nuernisha Alifu − *Department of Epidemiology and Health Statistics, School of Public Health, Xinjiang Medical University, Ürümqi 830054, China; State Key Laboratory of Pathogenesis, Prevention and Treatment of High Incidence Diseases in Central Asia, School of Medical Engineering and Technology, Xinjiang Medical University, Ürümqi 830054, China*; Email: nens_xjmu@126.com

Xueliang Zhang − *Department of Epidemiology and Health Statistics, School of Public Health, Xinjiang Medical University, Ürümqi 830054, China; State Key Laboratory of Pathogenesis, Prevention and Treatment of High Incidence Diseases in Central Asia, School of Medical Engineering and Technology, Xinjiang Medical University, Ürümqi 830054, China*; Email: shuxue2456@126.com

Authors

Ting Yan − *Department of Epidemiology and Health Statistics, School of Public Health, Xinjiang Medical University, Ürümqi 830054, China; State Key Laboratory of Pathogenesis, Prevention and Treatment of High Incidence Diseases in Central Asia, School of Medical Engineering and Technology, Xinjiang Medical University, Ürümqi 830054, China*

Gulinigaer Alimu − *Department of Epidemiology and Health Statistics, School of Public Health, Xinjiang Medical University, Ürümqi 830054, China; State Key Laboratory of Pathogenesis, Prevention and Treatment of High Incidence Diseases in Central Asia, School of Medical Engineering and Technology, Xinjiang Medical University, Ürümqi 830054, China*

Lijun Zhu − *Department of Epidemiology and Health Statistics, School of Public Health, Xinjiang Medical University, Ürümqi 830054, China; State Key Laboratory of Pathogenesis, Prevention and Treatment of High Incidence Diseases in Central Asia, School of Medical Engineering and Technology, Xinjiang Medical University, Ürümqi 830054, China*

Huimin Fan − *State Key Laboratory of Pathogenesis, Prevention and Treatment of High Incidence Diseases in Central Asia, School of Medical Engineering and Technology, Xinjiang Medical University, Ürümqi 830054, China*

Linxue Zhang − *State Key Laboratory of Pathogenesis, Prevention and Treatment of High Incidence Diseases in Central Asia, School of Medical Engineering and Technology, Xinjiang Medical University, Ürümqi 830054, China*; orcid.org/0000-0003-3452-2213

Zhong Du − *State Key Laboratory of Pathogenesis, Prevention and Treatment of High Incidence Diseases in Central Asia/Department of Gynecology, The First Affiliated Hospital of Xinjiang Medical University, Ürümqi 830054, China*

Rong Ma − *State Key Laboratory of Pathogenesis, Prevention and Treatment of High Incidence Diseases in Central Asia/Department of Gynecology, The First Affiliated Hospital of Xinjiang Medical University, Ürümqi 830054, China*

Shuang Chen − *State Key Laboratory of Pathogenesis, Prevention and Treatment of High Incidence Diseases in Central Asia/Department of Gynecology, The First Affiliated Hospital of Xinjiang Medical University, Ürümqi 830054, China*

Complete contact information is available at: https://pubs.acs.org/10.1021/acsomega.2c02977

Funding

The authors thank the Central Universities and State Key Laboratory of Pathogenesis, Prevention and Treatment of High Incidence Diseases in Central Asia Fund (SKL-HIDCA-2022-03).

Notes

The authors declare no competing financial interest.

■ ACKNOWLEDGMENTS

The authors are grateful to the valuable suggestion of Dr. N.A. and Dr. X.Z.

■ REFERENCES

(1) Hu, Z.; Ma, D. The precision prevention and therapy of HPV-related cervical cancer: new concepts and clinical implications. *Cancer Med.* **2018**, *7*, 5217−5236.

(2) Koh, W. J.; Abu-Rustum, N. R.; Bean, S.; Bradley, K.; Campos, S. M.; Cho, K. R.; Chon, H. S.; Chu, C.; Clark, R.; Cohn, D.; Crispens, M. A.; Damast, S.; Dorigo, O.; Eifel, P. J.; Fisher, C. M.; Frederick, P.; Gaffney, D. K.; Han, E.; Huh, W. K.; Lurain, J. R.; Mariani, A.; Mutch, D.; Nagel, C.; Nekhlyudov, L.; Fader, A. N.; Remmenga, S. W.; Reynolds, R. K.; Tillmanns, T.; Ueda, S.; Wyse, E.; Yashar, C. M.; McMillian, N. R.; Scavone, J. L. Cervical Cancer, Version 3.2019, NCCN Clinical Practice Guidelines in Oncology. *J. Natl. Compr. Cancer Network* **2019**, *17*, 64−84.

(3) Liontos, M.; Kyriazoglou, A.; Dimitriadis, I.; Dimopoulos, M. A.; Bamias, A. Systemic therapy in cervical cancer: 30 years in review. *Crit. Rev. Oncol./Hematol.* **2019**, *137*, 9−17.

(4) Feng, C. H.; Mell, L. K.; Sharabi, A. B.; McHale, M.; Mayadev, J. S.Immunotherapy With Radiotherapy and Chemoradiotherapy for Cervical Cancer. In *Seminars in Radiation Oncology*; WB Saunders, 2020; Vol. *30*, pp 273−280.

(5) Janicek, M. F.; Averette, H. E. Cervical cancer: prevention, diagnosis, and therapeutics. *Ca-Cancer J. Clin.* **2001**, *51*, 92−144.

(6) Mitra, A.; Grossman Biegert, G. W.; Delgado, A. Y.; Karpinets, T. V.; Solley, T. N.; Mezzari, M. P.; Yoshida-Court, K.; Petrosino, J. F.; Mikkelson, M. D.; Lin, L.; Eifel, P.; Zhang, J.; Ramondetta, L. M.;

Jhingran, A.; Sims, T. T.; Schmeler, K.; Okhuysen, P.; Colbert, L. E.; Klopp, A. H. Microbial Diversity and Composition Is Associated with Patient-Reported Toxicity during Chemoradiation Therapy for Cervical Cancer. *Int. J. Radiation Oncol., Biol., Phys.* **2020**, *107*, 163−171.
(7) Zhao, J.; Duan, L.; Wang, A.; Fei, J.; Li, J. Insight into the efficiency of oxygen introduced photodynamic therapy (PDT) and deep PDT against cancers with various assembled nanocarriers. *Wiley Interdiscip. Rev.: Nanomed. Nanobiotechnol.* **2020**, *12*, No. e1583.
(8) Liu, Q.; Tian, J.; Tian, Y.; Sun, Q.; Sun, D.; Liu, D.; Wang, F.; Xu, H.; Ying, G.; Wang, J.; Yetisen, A. K.; Jiang, N. Thiophene donor for NIR-II fluorescence imaging-guided photothermal/photodynamic/chemo combination therapy. *Acta Biomater.* **2021**, *127*, 287−297.
(9) Xu, P.; Liang, F. Nanomaterial-Based Tumor Photothermal Immunotherapy. *Int. J. Nanomed.* **2020**, *15*, 9159−9180.
(10) Ostańska, E.; Aebisher, D.; Bartusik-Aebisher, D. The potential of photodynamic therapy in current breast cancer treatment methodologies. *Biomed. Pharmacother.* **2021**, *137*, No. 111302.
(11) Zhou, Z.; Zhang, L.; Zhang, Z.; Liu, Z. Advances in photosensitizer-related design for photodynamic therapy. *Asian J. Pharm. Sci.* **2021**, *16*, 668−686.
(12) Gunaydin, G.; Gedik, M. E.; Ayan, S. Photodynamic Therapy-Current Limitations and Novel Approaches. *Front. Chem.* **2021**, *9*, No. 691697.
(13) Yan, J.; Wang, C.; Jiang, X.; Wei, Y.; Wang, Q.; Cui, K.; Xu, X.; Wang, F.; Zhang, L. Application of phototherapeutic-based nanoparticles in colorectal cancer. *Int. J. Biol. Sci.* **2021**, *17*, 1361−1381.
(14) Wu, W.; Shao, X.; Zhao, J.; Wu, M. Controllable Photodynamic Therapy Implemented by Regulating Singlet Oxygen Efficiency. *Adv. Sci.* **2017**, *4*, No. 1700113.
(15) da Silva, D. B.; da Silva, C. L.; Davanzo, N. N.; da Silva Souza, R.; Correa, R. J.; Tedesco, A. C.; Riemma Pierre, M. B. Protoporphyrin IX (PpIX) loaded PLGA nanoparticles for topical Photodynamic Therapy of melanoma cells. *Photodiagn. Photodyn. Ther.* **2021**, *35*, No. 102317.
(16) Ponce Ayala, E. T.; Alves Dias de Sousa, F.; Vollet-Filho, J. D.; Rodrigues Garcia, M.; de Boni, L.; Salvador Bagnato, V.; Pratavieira, S. Photodynamic and Sonodynamic Therapy with Protoporphyrin IX: In Vitro and In Vivo Studies. *Ultrasound Med. Biol.* **2021**, *47*, 1032−1044.
(17) Chudal, L.; Pandey, N. K.; Phan, J.; Johnson, O.; Li, X.; Chen, W. Investigation of PPIX-Lipo-MnO_2 to enhance photodynamic therapy by improving tumor hypoxia. *Mater. Sci. Eng.: C* **2019**, *104*, No. 109979.
(18) Chen, J.; Cui, Y.; Song, K.; Liu, T.; Zhou, L.; Bao, B.; Wang, R.; Wang, L. The self-assembly of a hybrid photosensitizer for the synergistically enhanced photodynamic/photothermal therapy. *Biomater. Sci.* **2021**, *9*, 2115−2123.
(19) Oh, J.; Yoon, H. J.; Park, J. H. Plasmonic liposomes for synergistic photodynamic and photothermal therapy. *J. Mater. Chem. B* **2014**, *2*, 2592−2597.
(20) Ma, R.; Alifu, N.; Du, Z.; Chen, S.; Heng, Y.; Wang, J.; Zhu, L.; Ma, C.; Zhang, X. Indocyanine Green-Based Theranostic Nanoplatform for NIR Fluorescence Image-Guided Chemo/Photothermal Therapy of Cervical Cancer. *Int. J. Nanomed.* **2021**, *16*, 4847−4861.
(21) Chen, Q.; Wen, J.; Li, H.; Xu, Y.; Liu, F.; Sun, S. Recent advances in different modal imaging-guided photothermal therapy. *Biomaterials* **2016**, *106*, 144−166.
(22) Liu, M.; Zhang, P.; Deng, L.; Guo, D.; Tan, M.; Huang, J.; Luo, Y.; Cao, Y.; Wang, Z. IR780-based light-responsive nanocomplexes combining phase transition for enhancing multimodal imaging-guided photothermal therapy. *Biomater. Sci.* **2019**, *7*, 1132−1146.
(23) Zhang, Y.; Wang, Q.; Ma, T.; Zhu, D.; Liu, T.; Lv, F. Tumor targeted combination therapy mediated by functional macrophages under fluorescence imaging guidance. *J. Controlled Release* **2020**, *328*, 127−140.
(24) Feng, Z.; Yu, X.; Jiang, M.; Zhu, L.; Zhang, Y.; Yang, W.; Xi, W.; Li, G.; Qian, J. Excretable IR-820 for in vivo NIR-II fluorescence cerebrovascular imaging and photothermal therapy of subcutaneous tumor. *Theranostics* **2019**, *9*, 5706−5719.
(25) Zhu, L.; Chen, J.; Yan, T.; Alimu, G.; Zhang, X.; Chen, S.; Aimaiti, M.; Ma, R.; Alifu, N. Near-infrared emissive polymer-coated IR-820 nanoparticles assisted photothermal therapy for cervical cancer cells. *J. Biophotonics* **2022**, *14*, No. e202200004.
(26) Jiang, Y.; Liu, Y.; Fang, S.; Ji, M. Gold Nanoshells Coated 5-Aminolevulinic Liposomes for Photothermal-Photodynamic Antitumor Therapy. *J. Nanosci. Nanotechnol.* **2020**, *20*, 1−14.
(27) Chen, W.; Goldys, E. M.; Deng, W. Light-induced liposomes for cancer therapeutics. *Prog. Lipid Res.* **2020**, *79*, No. 101052.
(28) Sonju, J. J.; Dahal, A.; Singh, S. S.; Jois, S. D. Peptide-functionalized liposomes as therapeutic and diagnostic tools for cancer treatment. *J. Controlled Release* **2021**, *329*, 624−644.
(29) Chen, Q.-B.; Shen, M.-H.; Ren, X.-H.; Zhu, S.; Shang, J.-T.; Liu, W.; Zhang, Z.-W.; Dong, Z.-J.; Gu, H.-Z.; Zhang, X.-Z.; Yuan, Q.; Zou, T. Tumor-triggered targeting ammonium bicarbonate liposomes for tumor multimodal therapy. *J. Mater. Chem. B* **2022**, *10*, 5154−5164.
(30) Taba, F.; Onoda, A.; Hasegawa, U.; Enoki, T.; Ooyama, Y.; Ohshita, J.; Hayashi, T. Mitochondria-Targeting Polyamine-Protoporphyrin Conjugates for Photodynamic Therapy. *ChemMedChem* **2018**, *13*, 15−19.
(31) Yu, Y.; Wang, B.; Guo, C.; Zhao, F.; Chen, D. Protoporphyrin IX-loaded laminarin nanoparticles for anticancer treatment, their cellular behavior, ROS detection, and animal studies. *Nanoscale Res. Lett.* **2019**, *14*, No. 316.
(32) Lu, H.; Wang, W.; Li, X.; Zhang, M.; Cheng, X.; Sun, K.; Ding, Y.; Li, X.; Hu, A. A carrier-free nanoparticle with dual NIR/acid responsiveness by co-assembly of enediyne and IR820 for combined PTT/chemotherapy. *J. Mater. Chem. B* **2021**, *9*, 4056−4064.
(33) Valcourt, D. M.; Dang, M. N.; Day, E. S. IR820-loaded PLGA nanoparticles for photothermal therapy of triple-negative breast cancer. *J. Biomed. Mater. Res., Part A* **2019**, *107*, 1702−1712.
(34) Yang, Y.; Wang, L.; Cao, H.; Li, Q.; Li, Y.; Han, M.; Wang, H.; Li, J. Photodynamic Therapy with Liposomes Encapsulating Photosensitizers with Aggregation-Induced Emission. *Nano Lett.* **2019**, *19*, 1821−1826.
(35) Temizel, E.; Sagir, T.; Ayan, E.; Isik, S.; Ozturk, R. Delivery of lipophilic porphyrin by liposome vehicles: preparation and photodynamic therapy activity against cancer cell lines. *Photodiagn. Photodyn. Ther.* **2014**, *11*, 537−545.
(36) Lin, X.; Cao, Y.; Xue, Y.; Wu, F.; Yu, F.; Wu, M.; Zhu, X. Multifunctional theranostic agents based on prussian blue nanoparticles for tumor targeted and MRI-guided photodynamic/photothermal combined treatment. *Nanotechnology* **2020**, *31*, No. 135101.
(37) Banerjee, M.; Pramanik, M.; Bhattacharya, D.; Lahiry, M.; Basu, S.; Chakrabarti, A. Faster heme loss from hemoglobin E than HbS, in acidic pH: effect of aminophospholipids. *J. Biosci.* **2011**, *36*, 809−816.
(38) Lei, H.; Guo, J.; Lv, Z.; Zhu, X.; Xue, X.; Wu, L.; Cao, W. Simultaneous Determination of Nitroimidazoles and Quinolones in Honey by Modified QuEChERS and LC-MS/MS Analysis. *Int. J. Anal. Chem.* **2018**, *2018*, No. 4271385.
(39) Alifu, N.; Ma, R.; Zhu, L.; Du, Z.; Chen, S.; Yan, T.; Alimu, G.; Zhang, L.; Zhang, X. A novel TMTP1-modified theranostic nanoplatform for targeted NIR-II fluorescence imaging-guided chemotherapy for cervical cancer. *J. Mater. Chem. B* **2022**, *4*, 506−517.
(40) Fan, H.; Chen, S.; Du, Z.; Yan, T.; Alimu, G.; Zhu, L.; Ma, R.; Alifu, N.; Zhang, X. New indocyanine green therapeutic fluorescence nanoprobes assisted high-efficient photothermal therapy for cervical cancer. *Dyes Pigm.* **2022**, *200*, No. 110174.
(41) Alifu, N.; Dong, X.; Li, D.; Sun, X.; Zebibula, A.; Zhang, D.; et al. Aggregation-induced emission nanoparticles as photosensitizer for two-photon photodynamic therapy. *Mater. Chem. Front.* **2017**, *1*, 1746−1753.
(42) Chen, Q.; He, S.; Zhang, F.; Cui, F.; Liu, J.; Wang, M.; Wang, D.; Jin, Z.; Li, C. A versatile Pt-Ce6 nanoplatform as catalase

https://doi.org/10.1021/acsomega.2c02977
ACS Omega 2022, 7, 44643−44656

nanozyme and NIR-II photothermal agent for enhanced PDT/PTT tumor therapy. *Sci. China Mater.* **2021**, *64*, 510−530.
(43) Chen, J.; Zhou, D.; Kang, J.; Liu, C.; Huang, R.; Jiang, Z.; Liao, Y.; Liu, A.; Gao, L.; Song, X.; Zhao, S.; Chen, Y.; Wang, H.; Lan, Z.; Wang, W.; Guan, H.; Chen, X.; Huang, J. ER stress modulates apoptosis in A431 cell subjected to EtNBSe-PDT via the PERK pathway. *Photodiagn. Photodyn. Ther.* **2021**, *34*, No. 102305.
(44) Ghafarkhani, M.; Avci, C. B.; Rahbarghazi, R.; Karimi, A.; Sadeghizadeh, M.; Zarebkohan, A.; Bani, F. Mild hyperthermia induced by gold nanorods acts as a dual-edge blade in the fate of SH-SY5Y cells via autophagy. *Sci. Rep.* **2021**, *11*, No. 23984.
(45) Li, G.; Song, Y. Z.; Huang, Z. J.; Chen, K.; Chen, D. W.; Deng, Y. H. Novel, nano-sized, liposome-encapsulated polyamidoamine dendrimer derivatives facilitate tumour targeting by overcoming the polyethylene glycol dilemma and integrin saturation obstacle. *J. Drug Targeting* **2017**, *25*, 734−746.
(46) Umar, A. K.; Sriwidodo, S.; Maksum, I. P.; Wathoni, N. Film-Forming Spray of Water-Soluble Chitosan Containing Liposome-Coated Human Epidermal Growth Factor for Wound Healing. *Molecules* **2021**, *26*, No. 5326.
(47) Huang, Y. S.; Hsu, W. C.; Lin, C. H.; Lo, S. N.; Cheng, C. N.; Lin, M. S.; Lee, T. W.; Chang, C. H.; Lan, K. L. Bi-Functional Radiotheranostics of Re-Liposome-Fcy-hEGF for Radio- and Chemo-Therapy of EGFR-Overexpressing Cancer Cells. *Int. J. Mol. Sci.* **2021**, *22*, No. 1920.
(48) Mohammed, Y.; Percy, A. J.; Chambers, A. G.; Borchers, C. H. Qualis-SIS: automated standard curve generation and quality assessment for multiplexed targeted quantitative proteomic experiments with labeled standards. *J. Proteome Res.* **2015**, *14*, 1137−1146.
(49) Yue, C.; Yang, Y.; Song, J.; Alfranca, G.; Zhang, C.; Zhang, Q.; Yin, T.; Pan, F.; de la, F. J. M.; Cui, D. Mitochondria-targeting near-infrared light-triggered thermosensitive liposomes for localized photothermal and photodynamic ablation of tumors combined with chemotherapy. *Nanoscale* **2017**, *9*, 11103−11118.
(50) Sumohan, P. A.; Alexander, A.; Sri, V. G.; Manikantan, V.; Allben, A. B.; Enoch, I. V. M. V. Poly-β-Cyclodextrin-coated neodymium-containing copper sulfide nanoparticles as an effective anticancer drug carrier. *J. Microencapsulation* **2022**, 1−26.
(51) Lismont, M.; Dreesen, L.; Heinrichs, B.; Paez, C. A. Protoporphyrin IX-Functionalized AgSiO Core-Shell Nanoparticles: Plasmonic Enhancement of Fluorescence and Singlet Oxygen Production. *Photochem. Photobiol.* **2016**, *92*, 247−256.
(52) Ding, M.; Shao, K.; Wu, L.; Jiang, Y.; Cheng, B.; Wang, L.; Shi, J.; Kong, X. NO/ROS/RNS cascaded-releasing nano-platform for gas/PDT/PTT/immunotherapy of tumors. *Biomater. Sci.* **2021**, *9*, 5824−5840.
(53) Xu, X.; Mao, H.; Wu, Y.; Liu, S.; Liu, J.; Li, Q.; Yang, M.; Zhu, J.; Zou, S.; Du, F. Fabrication of methylene blue-loaded ovalbumin/polypyrrole nanoparticles for enhanced phototherapy-triggered antitumour immune activation. *J. Nanobiotechnol.* **2022**, *20*, No. 297.
(54) Zhang, C.; Wu, J.; Liu, W.; Zhang, W.; Lee, C.; Wang, P. New Xanthene Dyes with NIR-II Emission Beyond 1200 nm for Efficient Tumor Angiography and Photothermal Therapy. *Small* **2022**, *18*, No. e2202078.
(55) Shan, X.; Zhang, X.; Wang, C.; Zhao, Z.; Zhang, S.; Wang, Y.; Sun, B.; Luo, C.; He, Z. Molecularly engineered carrier-free co-delivery nanoassembly for self-sensitized photothermal cancer therapy. *J. Nanobiotechnol.* **2021**, *19*, No. 282.
(56) Wang, X.; Zhang, H.; Bai, M.; Ning, T.; Ge, S.; Deng, T.; Liu, R.; Zhang, L.; Ying, G.; Ba, Y. Exosomes Serve as Nanoparticles to Deliver Anti-miR-214 to Reverse Chemoresistance to Cisplatin in Gastric Cancer. *Mol. Ther.* **2018**, *26*, 774−783.
(57) Xu, L.; Wang, J.; Lu, S. Y.; Wang, X.; Cao, Y.; Wang, M.; Liu, F.; Kang, Y.; Liu, H. Construction of a Polypyrrole-Based Multifunctional Nanocomposite for Dual-Modal Imaging and Enhanced Synergistic Phototherapy against Cancer Cells. *Langmuir* **2019**, *35*, 9246−9254.

https://doi.org/10.1021/acsomega.2c02977
ACS Omega 2022, 7, 44643−44656